Chapter

Nonlinear Frictional Dynamics on Rolling Contact

Yasunori Sakai

Abstract

The rolling machine element is indispensable for realizing high-precision and high-speed relative motion. In addition, its positioning accuracy is approaching the nanometer order, and its importance is expected to increase in the future. However, since the rolling elements and the raceways are mechanically in contact, various nonlinear phenomena occur. This complicated phenomenon must be clear by theoretically and experimentally. This chapter describes the nonlinear friction behavior occurred with rolling contact condition and its effect on the dynamics of bearings. First, the characteristics of the non-linear friction caused by rolling machine elements and the nonlinear friction modeling method using the Masing rule are described. From the numerical analysis using the friction model, it is clarified that the motion accuracy decreases due to sudden velocity variation caused by nonlinear friction. Also, the author show that the resonance phenomenon and force dependency of the dynamic characteristics of rolling machine element due to the nonlinear friction. Finally, the author indicates nonlinear friction influences on the dynamic characteristics in the directions other than the feed direction.

Keywords: nonlinear dynamics, friction, rolling machine element, elastic contact, bearing

1. Introduction

Rolling machine elements such as linear rolling bearings and rotational bearings are used in various industrial fields because they realize high precision relative motion at high speed. In addition, since the fluctuation of friction force is small, self-excited vibration called stick-slip is less likely to occur. Though rolling elements such as balls and rollers are always in point or line contact with the raceway, resulting in high surface pressure. The rolling contact condition complicates tribological phenomena such as friction and wear, and dynamic behavior of rolling machine elements.

Linear rolling bearings are widely used in semiconductor manufacturing equipment, ultra-precision positioning systems for machine tool, robots, and other equipment. Conventionally, it was necessary to use non-contact bearings such as hydrostatic linear guideways to achieve positioning with nanometer accuracy. However, it has become possible to achieve nanometer positioning accuracy even in rolling bearings by optimizing the rolling contact condition.

On the other hand, since rolling elements and raceways are in rolling contact with each other, the damping capacity of bearing is much lower than other guideways such as hydrostatic guides and sliding guides. In addition, the non-linear

behavior of contact friction produces resonance and displacement-amplitude dependency in the dynamics of bearings.

The resonance phenomenon of the bearing and the amplitude dependency of the dynamics lead to instability of the positioning control system and the deterioration of positioning accuracy [1–6]. In order to develop more accurate positioning control system and damping element for precision positioning system, it is important to clarify and model the effects of the nonlinear friction behavior on the dynamics of bearings.

This chapter describes the nonlinear friction behavior occurred with rolling contact condition and its effect on the dynamics of bearings. Section 2 explains the nonlinear spring behavior (NSB) depending on displacement, as well as the modeling method of the nonlinear frictional behavior. Section 3 describes the influence of nonlinear friction on the dynamics of the bearing with some numerical and experimental results. Section 4 shows the influence of nonlinear friction on the dynamics in directions other than the feed direction of the bearing. Section 5 concludes the chapter and gives the future interest of the research related to rolling friction behavior.

2. Nonlinear friction behavior in microscopic displacement regime

2.1 Displacement dependent nonlinearity

Figure 1 shows the relationship between the friction force F of the sliding object and its translational displacement x [7]. After the mass is starting motion, the friction force increases as the displacement increases. When the friction force is saturated with the steady state friction force F_s, it is constant until the mass reaches the reversal point A. After reversing the direction of motion at point A, the friction force changes along the outer hysteresis curve ABA. If the motion is reversed at arbitrary point a on the outer hysteresis curve, the friction force will change along the inner hysteresis curve aba starting at point a. When the internal hysteresis curve is closed, the frictional force changes along ABA again. This hysteresis rule is known as the non-local memory NSB [8]. The NSB is caused by elastic deformation of the contact surface asperities [9], microslip [10], and elastic hysteresis loss [11]. In this chapter, the curve OA is called a virgin loading curve, the displacement region where the friction depends on the displacement is called the pre-rolling region, and the displacement region where the friction force is constant is called the rolling

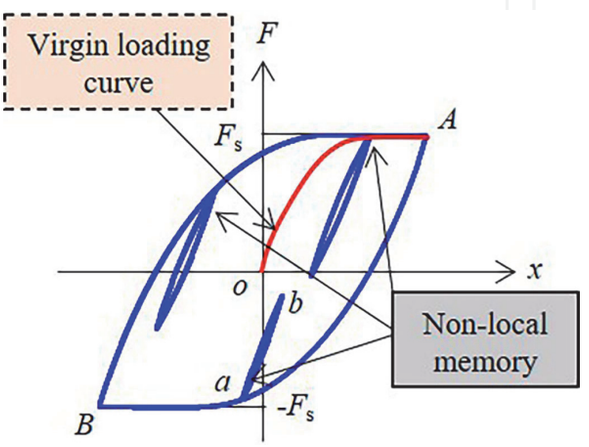

Figure 1.
The relationship between the friction force F *and the displacement* x.

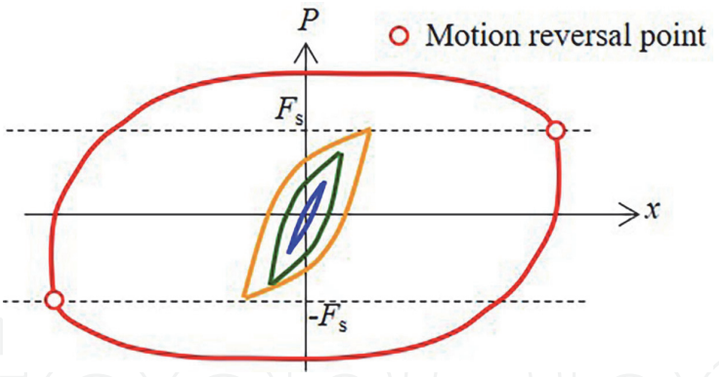

Figure 2.
The relationship between the sinusoidal excitation force P *and the displacement* x.

region. Furthermore, the boundary displacement between the pre-rolling region and the rolling region is called the starting rolling displacement.

Now, the sinusoidal excitation force $P(t) = P_0 \sin\omega t$ acting on the mass where P_0 is the amplitude and ω is the excitation angular frequency. **Figure 2** shows the relationship between sinusoidal excitation force P and displacement x [7]. If the force amplitude P_0 is greater than the static friction force F_s, the displacement will change significantly (such as an arc within $P > F_s$). This suggests that the rolling element initiates a rolling movement. F_s can be determined as P at the motion reversal point [12].

2.2 Nonlinear friction modeling

The friction model proposed based on the Masing rule can describe the NSB and hysteresis behavior of friction in non-local memory. The Masing rule simply describes a hysteresis curve from the virgin loading curve. Therefore, it is widely used in the basic model of seismic response analysis [13] and the hysteresis model [14]. The Masing rule is formulated as follows:

$$F = \begin{cases} f(x) & (x \geq 0) \\ -f(-x) & (x < 0) \end{cases} \tag{1}$$

$$F = \begin{cases} F_r + \lambda f\left(\dfrac{x - x_r}{\lambda}\right) & \left(\dfrac{x - x_r}{\lambda} \geq 0\right) \\ F_r - \lambda f\left(-\dfrac{x - x_r}{\lambda}\right) & \left(\dfrac{x - x_r}{\lambda} < 0\right) \end{cases} \tag{2}$$

where $f(x)$ is the virgin loading curve. F_r and x_r are the friction force and displacement at the motion reversal point. The hysteresis curve is determined by the geometrically similar curve of the virgin loading curve with a similarity ratio $\lambda = 2$. If $\lambda \neq 2$, the hysteresis curve does not become axisymmetric. In the friction model, $\lambda = 2$.

Figure 3 shows the procedure for calculating the friction force [7]. First, the friction force is calculated by Eq. (1) until reaching the motion reversal point A. After reversing the direction of motion at point A, calculate the friction force using Eq. (2). At this time, the values of x_r and F_r are replaced by the displacement and frictional force at point A. Furthermore, the friction force can be calculated as well when the motion is reversed at the point B or C. The friction force after closing the

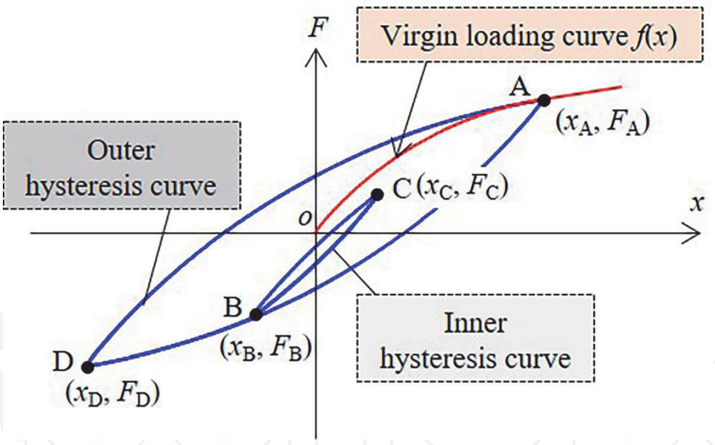

Figure 3.
The relation between friction force F *and displacement* x *calculated by Masing rule.*

internal hysteresis curve aba is calculated with Eq. (2) by replacing the values of x_r and f_r to the displacement and friction at point A.

The hysteresis characteristics of non-local memory can be explained by above mentioned calculations. If x is greater than the maximum displacement value at the previous motion reversal point, the frictional force is calculated by Eq. (1) again.

This model has fewer parameters than previous friction models such as the bristle model [15] and the generalized Maxwell slip (GMS) model [16].

The friction model based on the Masing rule can describe the effect of NSB on the dynamic characteristics by simplifying the friction behavior. Al-Bender uses the exponential and irrational functions as the virgin loading curves to calculate the friction force [17]. However, the rolling region and the starting rolling displacement x_s do not consider. The resonances caused by NSB are depended on x_s [18]. Therefore, the starting rolling displacement and steady-state friction force in the rolling region should be introduced into the friction model.

The virgin loading curve is described by Eq. (3) proposed in this study:

$$f(x) = \begin{cases} A(x + Bx^n) \equiv f_1(x) & (x \le x_s) \\ F_s \equiv f_2(x) & (x > x_s) \end{cases} \tag{3}$$

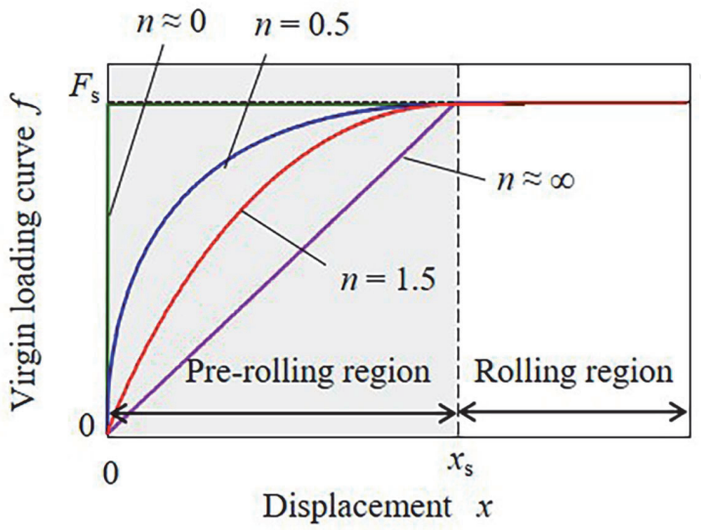

Figure 4.
The proposed virgin loading curve f *for different shape factor* n.

where A and B are constants determined by the continuity condition as below:

$$f_1(x_s) = f_2(x_s) \tag{4}$$

$$\left.\frac{df_1(x)}{dx}\right|_{x=x_s} = \left.\frac{df_2(x)}{dx}\right|_{x=x_s} \tag{5}$$

This virgin loading curve has only three parameters: steady-state friction force F_s, starting rolling displacement x_s, and shape factor n. The shape factor n represents the rate of change in friction of the pre-rolling region and is the most important parameter in this model [19]. These parameters determine the characteristics of the NSB. The proposed virgin loading curves for different n are shown in **Figure 4** [7].

In this model, $n \neq 1$ is always satisfied. Because $n = 1$ means that the friction does not have hysteretic behavior, it is uncommon in the friction characteristics of a rolling bearing.

3. Resonance phenomenon caused by nonlinear frictional behavior

In this section, the frictional effect of NSB on the dynamic characteristics of the sliding object is discussed. The frequency response of the sliding object is an important consideration for developing a highly accurate feed drive system in machine tool and precision machines using friction compensators.

3.1 Numerical analysis of dynamics considering nonlinear friction

Figure 5 shows an analytical model for calculating the dynamics in the feed direction [7]. The equation of motion is as follows:

$$m\ddot{x} = -F(x) + P(t) \tag{6}$$

where m is the mass of sliding object; t is the time; $[\cdot] = d/dt$; $P(t)$ is the exciting force acting on the mass; $F(x)$ is the friction force calculated from Eqs. (1)–(3).

The equation of motion can be expressed by Eq. (7) considering the sinusoidal excitation force $P(t) = P_0 \sin\omega t$ acting on the mass.

$$m\ddot{x} = -F(x) + P_0 \sin \omega t \tag{7}$$

By introducing the dimensionless parameters $K_s = F_s/x_s$, $\omega_s{}^2 = K_s/m$, $u = x/x_s$, $\gamma_0 = P_0/F_s$, $\tau = \omega t$, $\beta = \omega/\omega_s$ and $[\text{'}] = d/d\tau$ into the Eq. (7), the dimensionless equation of motion is described as Eq. (8).

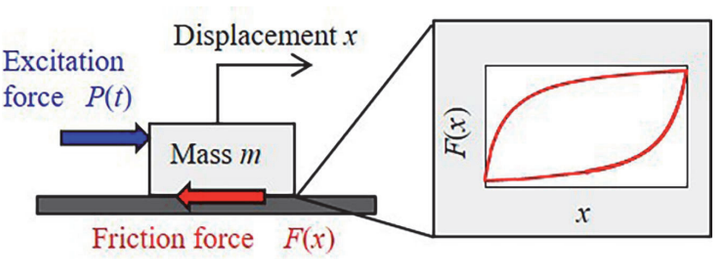

Figure 5.
The analytical model of the rolling guideway for calculating the dynamic characteristics in the feed direction in consideration of the nonlinear spring behavior of friction.

$$\beta^2 u'' = -\frac{F(u)}{F_s} + \gamma_0 \sin\tau \tag{8}$$

As shown in Eq. (8), the motion of the sliding object is governed by the amplitude of the dimensionless excitation force γ_0, the dimensionless excitation frequency β, and the dimensionless friction force F/F_s. F/F_s is a function of shape factor n. Ultimately, the motion of the sliding object is described by determining γ_0, β, and n. Eq. (8) is solved by the fourth-order Runge-Kutta method with nondimensional time derivative $d\tau = \tau/10000$. The frequency response function (FRF) $G(\beta)$ is calculated by Eq. (9).

$$G(\beta) = \frac{u_0}{\gamma_0} = \frac{(u_{\max} - u_{\min})}{2\gamma_0} \tag{9}$$

where u_0 is the displacement amplitude in the steady-state response, $u_{\max}$ and $u_{\min}$ are the maximum and minimum displacements in the steady-state response, respectively.

Figure 6 shows an FRF with dimensionless excitation force amplitude $\gamma_0 = 0.6$ for $n = 0.5$ and 1.5 [7]. As shown in **Figure 6**, the FRF shape and resonant frequency change by n. It means that the NSB affects the dynamic characteristics of the sliding object. There are additional small resonant peaks in the FRF. The small resonance peaks are superharmonic resonances, which are typical phenomenon of nonlinear vibration caused by the nonlinearity of restoring forces [20]. Because the proposed friction model does not take into account the difference between static and dynamic friction, these resonances does not induced by the stick-slip phenomena which is occurred by the negative damping due to the difference between static and dynamic friction forces. In the following, the main resonance peaks are called harmonic resonances and the other resonances are called superharmonic resonances.

By calculating the steady-state response of a specific excitation frequency, the effect of the excitation frequency on the steady-state motion in the feed direction is clarified. **Figures 7–9** show the phase planes of the limit cycles of $n = 0.5$ and 1.5 at frequencies A, B, and C shown in **Figure 6**, respectively [7]. Frequency A is lower than the frequency of the superharmonic resonance of the adjacent harmonic resonance. Frequency B lies between the harmonic resonance and its adjacent superharmonic resonance. Finally, frequency C is higher than the frequency of harmonic resonance.

According to the results as shown in **Figure 7**, when a sliding object is excited by a sinusoidal force of frequency A, velocity reduction and recovery (VRAR) occurs

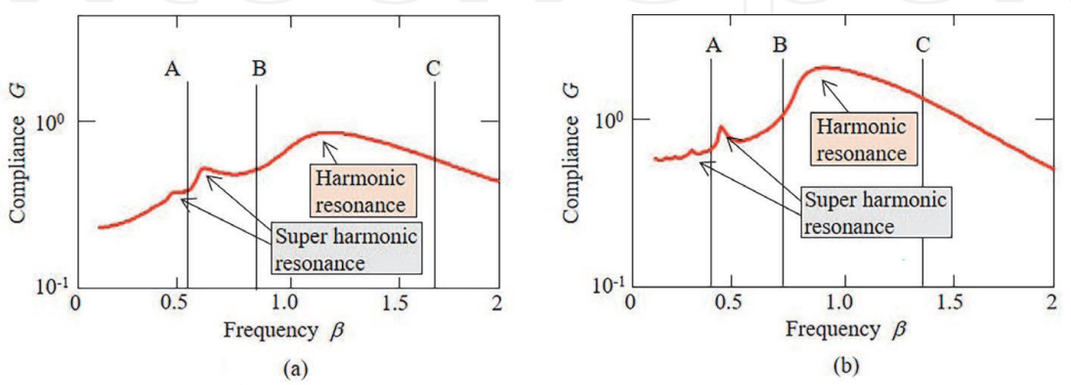

Figure 6.
The frequency response functions in the feed direction with the non-dimensional excitation force amplitude $\gamma_0 = 0.6$ for different shape factor n. *(a)* n = *0.5. (b)* n = *1.5.*

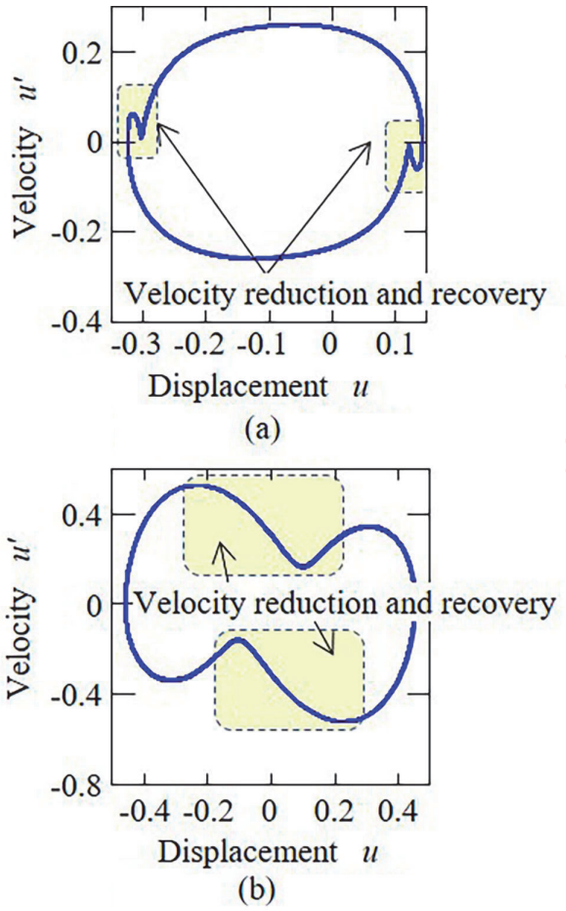

Figure 7.
The phase plane at frequency of A. (a) n = *0.5*, β = *0.54. (b)* n = *1.5*, β = *0.45.*

after reversing the direction of movement. When the sliding object is excited at frequency B, VRAR does not occur after reversing the direction of movement, as shown in **Figure 8**. However, the shape of the phase plane is distorted. On the other hand, as shown in **Figure 9**, when the sliding object is excited at frequency C, the phase plane becomes circular. If the sliding object is excited by a force with a frequency higher than the harmonic resonance, the non-linearity due to NSB is negligible.

Next, the effect of excitation and friction conditions on the time history of steady-state motion is examined. **Figures 10** and **11** show the dimensionless acceleration u , dimensionless velocity u', dimensionless displacement u, and dimensionless friction force F/F_s at frequencies A and B with n = 0.5 and 1.5, respectively [7].

Comparing **Figures 10** and **11**, the variation of acceleration direction (VOAD) unrelated to sinusoidal displacement motion with the excitation frequency and VRAR are clear when excited with frequency A. Hence, the VOAD causes VRAR. The displacement spike is clearly observed in **Figure 10**, but it does not observe in **Figure 11**. Thus, the displacement spike is caused by the VOAD. Furthermore, the displacement spike sharpens when the VOAD is caused discontinuously. On the other hand, it loosens when the VOAD is caused continuously. The VOAD is affected by NSB of friction and becomes discontinuous when n is small.

Displacement spikes, known as quadrant glitches, are one of the causes of poor feed drive operation accuracy. Previous studies have concluded that quadrant glitches are produced due to motion delays caused by the difference between static and dynamic friction [21]. The results of this study show that displacement spikes

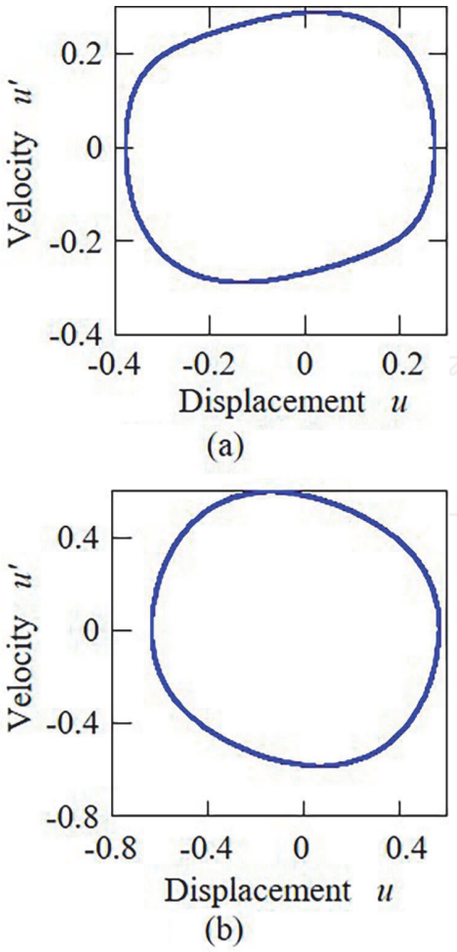

Figure 8.
The phase plane at frequency of B. (a) n = *0.5*, β = *0.90. (b)* n = *1.5*, β = *0.71.*

(quadrant glitches) are generated without modeling the difference between static and dynamic frictional forces. It means that the quadrant glitches are caused not only by the difference between static and dynamic friction, but also by NSB friction. Also, as shown in **Figure 10**, the quadrant glitches occur even at zero speed. Previous studies have concluded that quadrant glitches are produced by reduced acceleration [22]. These conclusions correspond to our result that quadrant glitches are caused by VOAD.

Figure 12 shows the FRF for n = 0.5 and 1.5. The figure also contains the results of various dimensionless excitation force amplitudes γ_0 [7]. As shown in **Figure 12**, as γ_0 increases, the resonant frequency decreases. Furthermore, resonance does not occur even if γ_0 increases. The compliance at frequencies of superharmonic and harmonic resonance increases with higher values of n. For small n, not only the nonlinearity but also the damping increases. Therefore, when n is small, the compliance at resonance is not high than the case with large n.

Then, the results of the proposed friction model are compared with the experimental results using commercially available roller guideways for verifying the validity.

Figure 13 shows the relationship between the excitation force amplitude and the frequency and compliance at the harmonic resonance [7]. **Figure 13** shows the measurement results of the compliance in the feed direction of the linear rolling bearing obtained in the vibration test conducted under the same conditions as the numerical analysis. The analytical results for n = 1.5 conform well to the experimental results. The comparison results prove that the proposed simple analytical

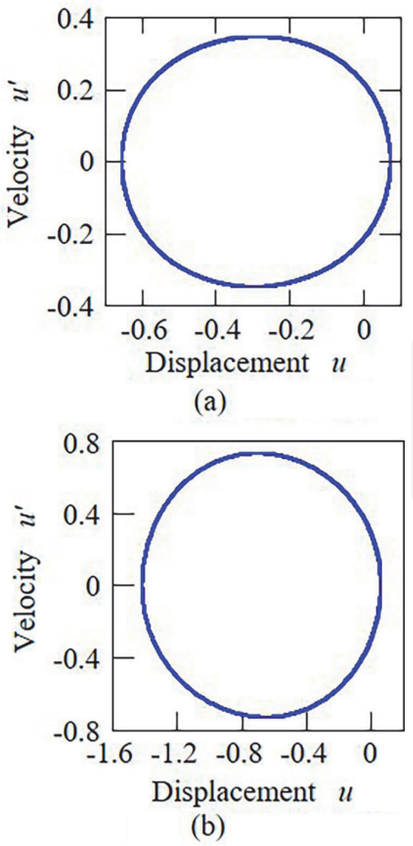

Figure 9.
The phase plane at frequency of C. (a) n = 0.5, β = 1.65. *(b)* n = 1.5, β = 1.40.

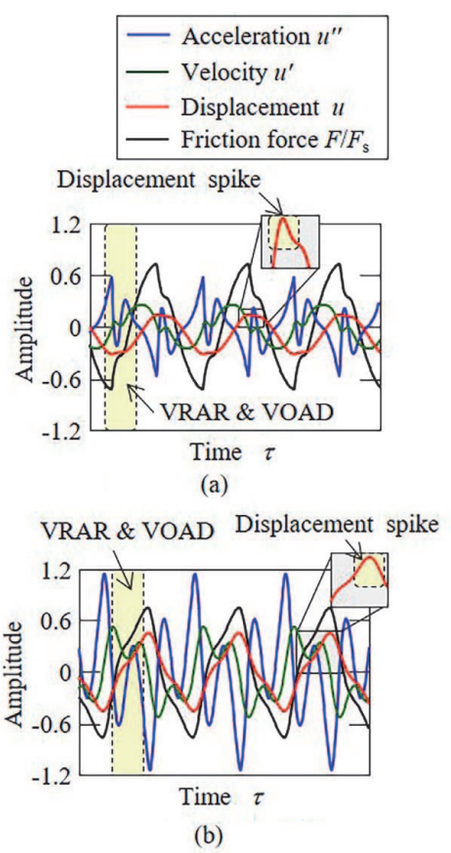

Figure 10.
Time history at the frequency of A. (a) n = 0.5, β = 0.54. *(b)* n = 1.5, β = 0.45.

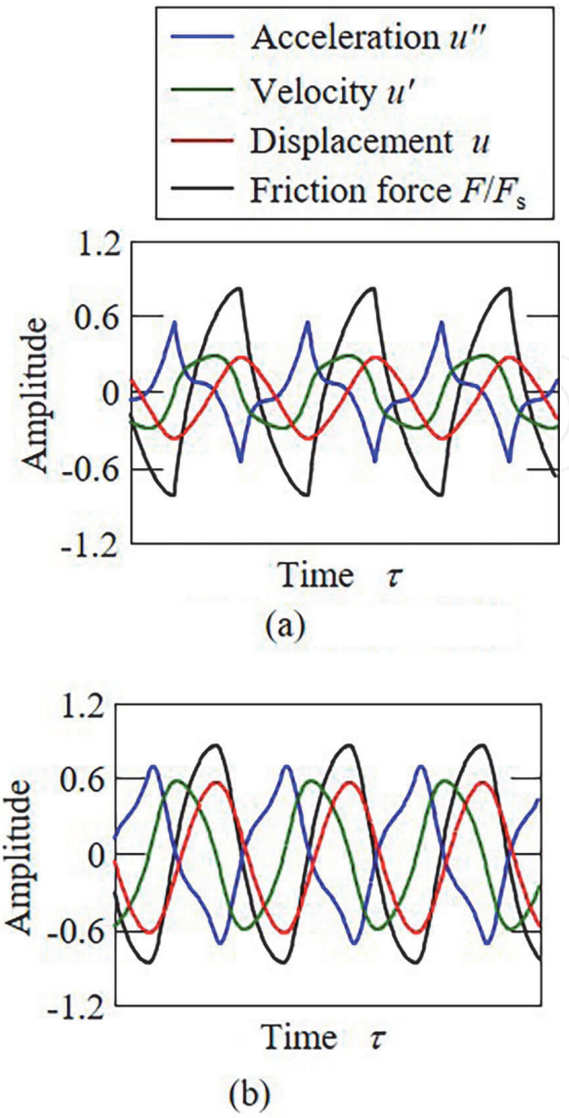

Figure 11.
Time history at the frequency of B. (a) n = 0.5, β = 0.90. *(b)* n = 1.5, β = 0.71.

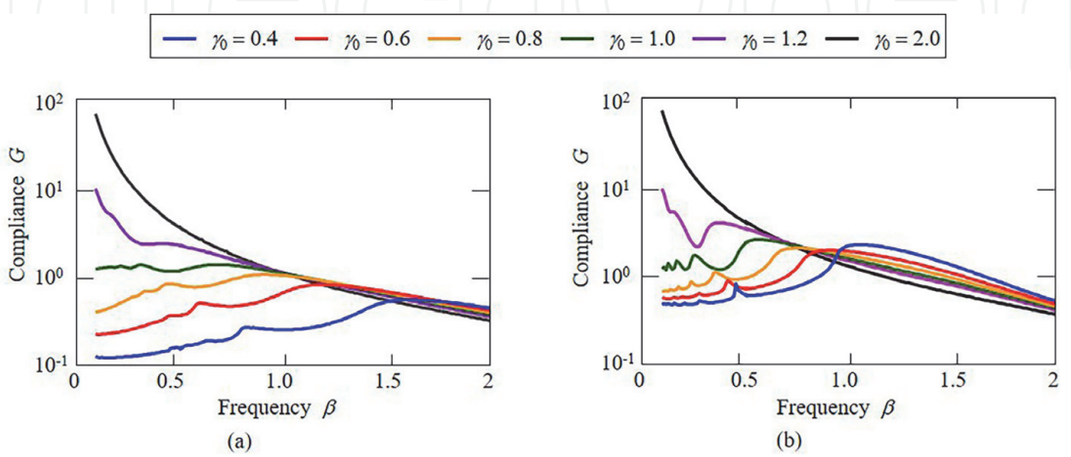

Figure 12.
The force amplitude dependency of the frequency response caused by the nonlinear spring behavior. (a) n = 0.5. *(b)* n = 1.5.

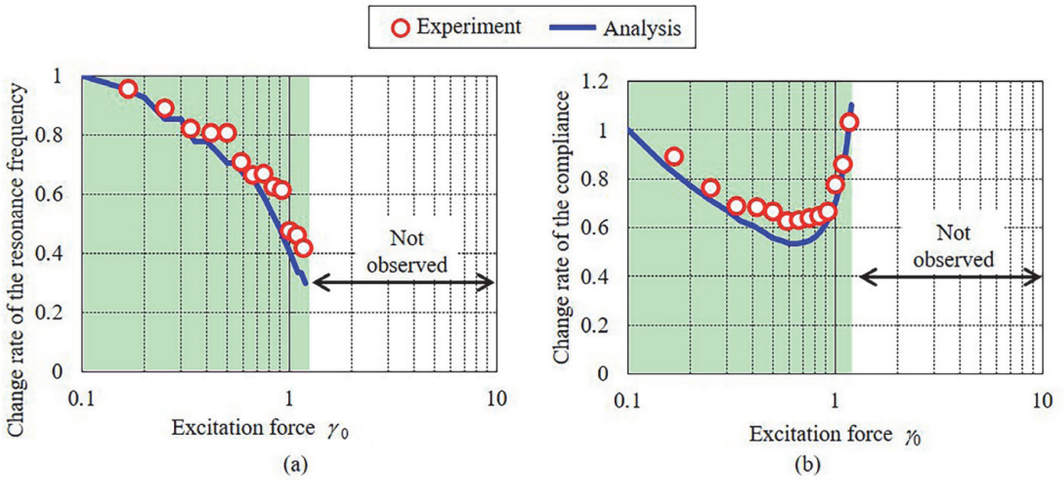

Figure 13.
Relationship between the non-dimensional excitation force amplitude γ_0 and the resonance frequency and compliance at the harmonic resonance. (a) Harmonic resonance frequency. (b) Compliance at the harmonic resonance.

model can qualitatively predict the force dependency of the dynamic characteristics of a rolling bearing in the feed direction.

4. Nonlinear behavior of rotational direction induced by friction

4.1 Experiment for evaluating the dynamics of linear rolling bearing

In a previous study, Yi et al. evaluated the vibration characteristics of a carriage with a steel block (additional mass). Feed, lateral, and vertical response accelerations were measured using a 3-axis accelerometer when the steel block was excited by the shaker [23]. Ota et al. measured the vibration of the carriage moving at a constant speed in the feed direction. They also identified key vibrational components by frequency spectrum analysis of the detected response sounds and accelerations [24]. Through the impulse hammering test, Rahman et al. evaluated the natural frequencies and damping ratios of machine tool tables supported by linear rolling bearings. The natural frequency and damping ratio were identified based on the frequency response function [25].

In contrast, the author measured the acceleration of a carriage carrying a column which is imitated the long workpiece. The vibration measuring system for evaluating the dynamic characteristics of the linear rolling bearing is shown in **Figure 14** [26]. The system comprises a rail, a carriage, a column made of S50C steel, an electrodynamic shaker, and a stinger made of S45C. The column was fixed on the carriage with bolts. The rail was fixed on the stone surface plate through the steel base. The shaker was supported with cloth belt to obtain a free boundary condition. The stinger has a circular cross-sectional shape. One of stinger ends was screwed to the free end of the column through the impedance head, and the other one was screwed to the shaker.

The column was used as a pseudo workpiece to satisfy the condition that the center of gravity is higher than the upper surface of the carriage. This condition is often observed in the general usage of linear rolling bearings, such as in the feed drive mechanism of a machine tool. The excitation force in the feed direction was applied to the free end of the column.

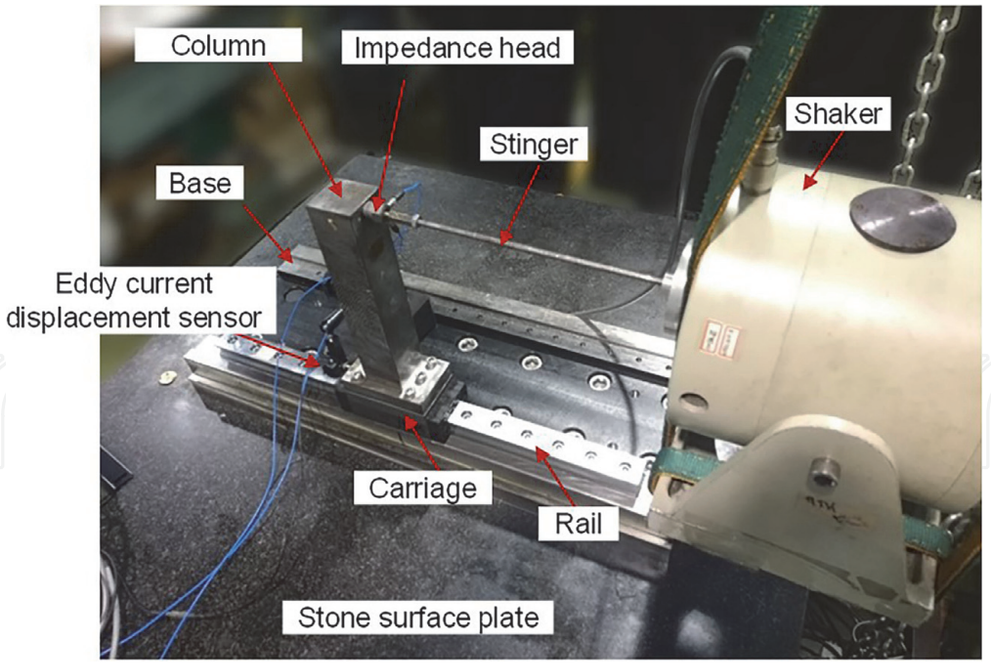

Figure 14.
Experimental setup for evaluating the vibration characteristics.

The sinusoidal excitation signal generated using the function generator was input to the shaker via a power amplifier. The excitation and acceleration signals detected at the free end of the column were amplified by a charge amplifier and analyzed using a digital spectrum analyzer. In addition, at the same time as the excitation, the eddy current displacement sensor was used to detect the response displacement of the carriage in the feed direction.

In the general case, forces with different amplitudes and frequencies act on the linear rolling guide. For example, in the case of a machine tool, cutting force acts on the rolling guide via the workpiece and table. Its frequency and amplitude vary widely depending on machining conditions such as depth of cut and spindle speed. Micro cutting exerts a force of several millinewtons, and heavy cutting exerts a force of hundreds of newtons. Therefore, the exciting force changed from 0.1 N to 100 N in half amplitude and up to 1000 Hz in frequency.

The lubricant (mineral oil) weighed by syringe was manually applied to the raceways (5 ml per raceway). When changing the lubricant oil, the all components of the linear rolling bearing were washed with kerosene and alcohol for degreasing.

4.2 Influence of excitation force in rotational direction

Figure 15 shows the FRF when excited in the feed direction. Two resonance peaks were observed in the FRF [26]. The vibration modes at these resonance frequencies were measured by experimental modal analysis. **Figure 16** shows the mode shapes of the carriage and column at the two resonances [26]. At the lower resonance frequency, the carriage and column vibrate in the feed direction without any elastic deformation. It was caused by the nonlinear spring behavior of friction in the microscopic region discussed in the previous chapters. At the higher resonance frequency, the carriage and column vibrated in the pitch direction. This natural vibration is caused by the elastic deformation of the contact part between the raceways and the rollers. Since the center of gravity is higher than the upper surface of the carriage, not only the pitching motion but also the translational motion in the feed direction is occurred at the same time. In followings, these

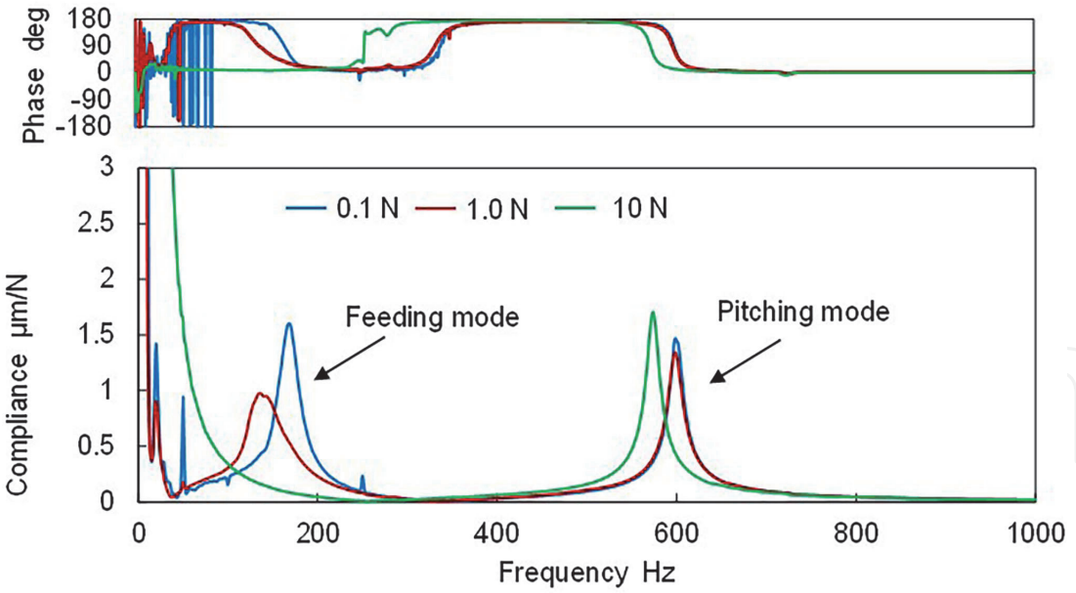

Figure 15.
Force amplitude dependency of dynamic characteristics.

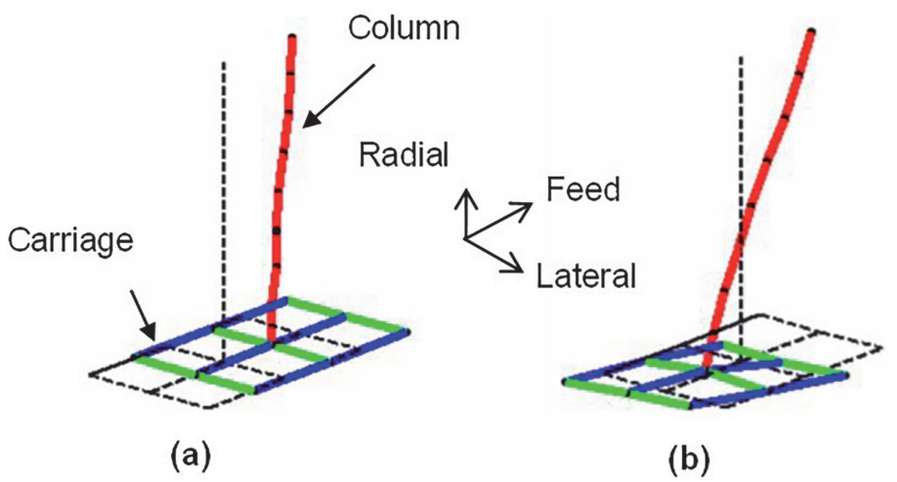

Figure 16.
Measured natural vibration modes of causing each resonance peaks in FRF. (a) Feeding mode. (b) Pitching mode.

vibration modes are called "feed mode" and "pitching mode" in order from low frequency.

Figure 15 also shows the FRFs for different excitation force amplitude. As shown in figure, the dynamic characteristics of the linear rolling bearing change depending on the exciting force. In feed mode, the resonance frequency decreased as the excitation force amplitude increased. Eventually, the feeding mode became unobservable as the excitation force became large. The resonant peak due to the pitching mode has the same tendency as the feed mode for the excitation force amplitude. However, even if the exciting force became large, the resonance peak did not disappear.

Pitching mode is the natural vibration by the rigid body motion of the carriage due to elastic deformation at the contact point between the roller and the raceway.

In the previous study, Ota et al. used a single carriage model to analyze the resonant frequency in pitching mode [27]. In their case, the center of gravity was close to the center of the rail cross section, and the natural vibration characteristics were determined based on the stiffness of the contact parts. However, under actual

usage conditions of linear rolling bearings, the center of gravity is higher than the top surface of the carriage. As a result, the natural vibration characteristics are affected by nonlinear friction. The carriage rotates around the center of gravity like a cradle and moves slightly in the feed direction.

In this state, the natural vibration characteristics of the pitching mode depend on the exciting force as shown in **Figure 16**, which is due to the influence of the nonlinear spring behavior.

As shown in the **Figure 17**, the resonance frequency of the pitching mode becomes high when the excitation force is small [26]. This indicates that frictional stiffness affects the pitching mode as "additional spring." Considering the feed mode, the resonance peak disappeared because of an increase in the excitation force amplitude. It indicates that the influence of the nonlinear spring behavior of friction decreases as the response displacement amplitude increases. Thus, the influence of nonlinear friction on the dynamic characteristics of pitching mode becomes small. In addition, the damping ratio was constant in the small excitation force range up to

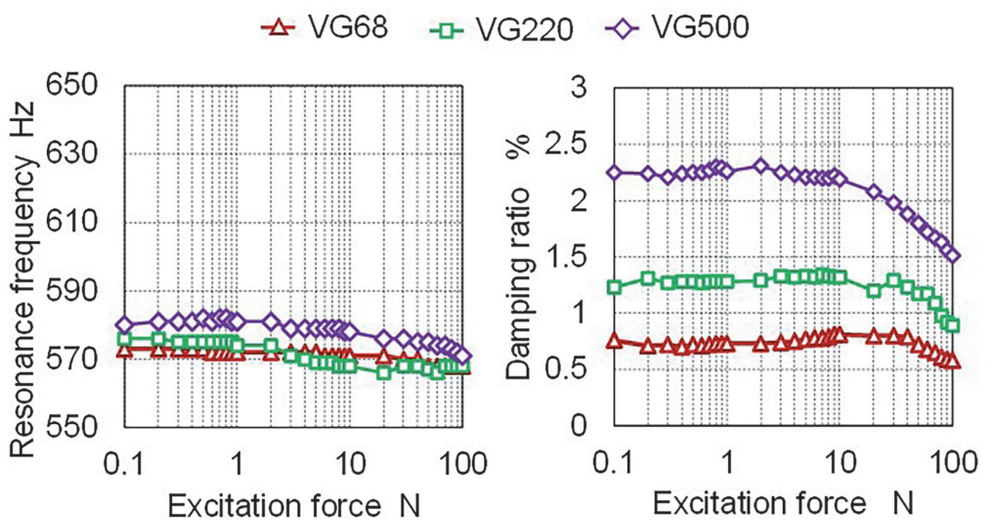

Figure 17.
Influence of oil specification on the nonlinearity of natural vibration characteristics in the pitching mode.

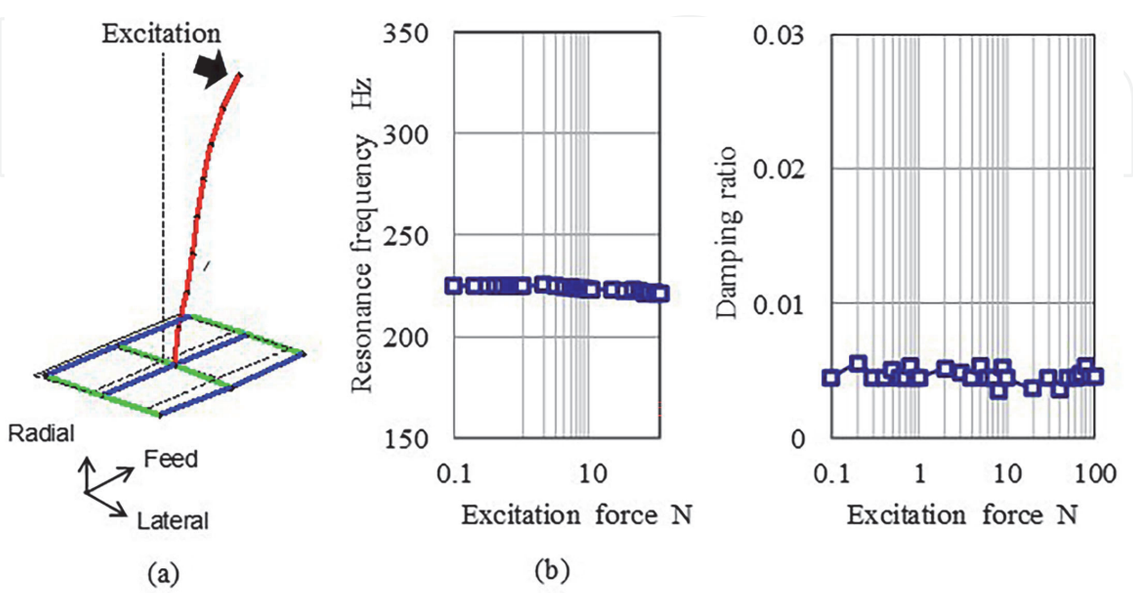

Figure 18.
Influence of excitation force amplitude on the nonlinearity of natural vibration characteristics in the rolling mode. (a) Rolling mode. (b) Dynamic characteristics of rolling mode.

about 10 N, but it decreased in the large excitation force range. According to our previous research, the damping ratio of the linear rolling guideway estimated by the impulse test with 2000 N in the excitation force was about 0.5% with a nonlubricated condition [28]. Thus, the damping ratio converged to about 0.5% when the excitation force increased further.

Figure 17 also shows the results when three types of oils with different kinematic viscosities are used. If the higher kinematic viscosity oil was used, the resonance frequency became higher. The frictional stiffness is high when oil with a high kinematic viscosity is used. These results indicate the difference in the resonance frequency of the pitching mode caused by frictional effect. The damping ratio tends to be higher when oil with higher kinematic viscosity is used. This means that the viscous damping due to the oil film was dominant in the pitching mode.

On the other hand, when the column is excited in the lateral direction, the rolling mode which the carriage and column vibrate around feed axis as shown in **Figure 18** was occurred. However, the excitation force dependence seen in the pitching mode does not occur. This is because the rolling mode is not affected by the additional spring due to non-linear friction.

5. Conclusions

The rolling machine element is indispensable for realizing high-precision and high-speed relative motion. In addition, its positioning accuracy is approaching the nanometer order, and its importance is expected to increase in the future.

However, since the rolling elements and the raceways are mechanically in contact, various non-linear phenomena occur. This complicated phenomenon has to be clear by theoretically and experimentally. In this chapter, the author explained the nonlinear spring behavior of friction that occurs in the rolling contact state and its modeling method. Furthermore, the effect of nonlinear friction on the dynamic characteristics of sliding objects was analyzed numerically. The validity of the model was verified by comparing with the experimental results using the rolling guide.

Finally, it was experimentally shown that the nonlinearity of rolling friction affects the motion in directions other than the feed direction. It is known that rolling friction has velocity dependence and acceleration dependence in addition to the nonlinear spring behavior described in this chapter.

Acknowledgements

This work was supported by Japan Society for Promotion of Science (JSPS) KAKENHI Grant Numbers JP16K21036, JP15J06292.

Nomenclature

A, B	constants
f	virgin loading curve
f_1	proposed virgin loading curve in the pre-rolling region
f_2	proposed virgin loading curve in the rolling region
F	friction force
F_r	friction force at the arbitrary motion reversal point
F_s	steady-state friction force

G	nondimensional compliance, u_0/γ_0
K_s	stiffness at the starting rolling displacement, F_s/x_s
m	mass of a carriage
n	change rate of the friction in the pre-rolling region
P	excitation force acting on the carriage
P_0	sinusoidal excitation force amplitude
t	time
u	nondimensional displacement, x/x_s
u_{max}	maximum nondimensional displacement in the steady-state response
u_{min}	minimum non-dimensional displacement in the steady-state response
u_0	nondimensional displacement amplitude in the steady-state response
x	displacement of the carriage in the feed direction
x_r	displacement at the arbitrary motion reversal point
x_s	starting rolling displacement
β	nondimensional frequency, ω/ω_s
dt	time differential
$d\tau$	nondimensional time differential
γ_0	nondimensional amplitude of the sinusoidal excitation force
λ	similarity ratio
ω	sinusoidal excitation force frequency
ω_s	natural angular frequency at the starting rolling displacement, K_s/m
τ	nondimensional time, ωt
$[\dot{}]$	differential operator with respect to time t, d/dt
$[']$	differential operator with respect to nondimensional time τ, $d/d\tau$

Author details

Yasunori Sakai
Shibaura Institute of Technology, Saitama, Japan

*Address all correspondence to: sakaiy@shbaura-it.ac.jp

References

[1] Rivin Eugene I. , Author, Balachandran B. , Reviewer. Stiffness and Damping in Mechanical Design. J Mech Des [Internet]. 2000 Mar 1;122 (1):147. Available from: https://doi.org/10.1115/1.533570

[2] Altintas Y, Verl A, Brecher C, Uriarte L, Pritschow G. Machine tool feed drives. CIRP Ann - Manuf Technol [Internet]. 2011;60(2):779–96. Available from: http://dx.doi.org/10.1016/j.cirp.2011.05.010

[3] Majda P. Modeling of geometric errors of linear guideway and their influence on joint kinematic error in machine tools. Precis Eng [Internet]. 2012;36(3):369–78. Available from: http://dx.doi.org/10.1016/j.precisioneng.2012.02.001

[4] Feng G, Wang C. Examining the misalignment of a linear guideway pair on a feed drive system under different ball screw preload levels with a cost-effective MEMS vibration sensing system. Precis Eng [Internet]. 2017;50:467–81. Available from: http://dx.doi.org/10.1016/j.precisioneng.2017.07.001

[5] Hung J, Lai Y, Lin C, Lo T. Modeling the machining stability of a vertical milling machine under the influence of the preloaded linear guide. Int J Mach Tools Manuf [Internet]. 2011;51(9):731–9. Available from: http://dx.doi.org/10.1016/j.ijmachtools.2011.05.002

[6] Wu JS, Chang J, Tsai G, Lin C, Ou F. The effect of bending loads on the dynamic behaviors of a rolling guide. J Mech Sci Technol. 2012;26(3):671–80.

[7] SAKAI Y, TANAKA T, YOSHIOKA H, ZHU J, TSUTSUMI M, SAITO Y. Influence of nonlinear spring behavior of friction on dynamic characteristics of a rolling guideway. J Adv Mech Des Syst Manuf. 2015;9(1):JAMDSM0004–JAMDSM0004.

[8] Al-bender F. Fundamentals of Friction Modeling. In: Proceedings, ASPE Spring Topical Meeting on Control of Precision Systems,. 2010. p. 117–22.

[9] Kenneth Langstreth Johnson. Surface interaction between elastically loaded bodies under tangential forces. Proc R Soc London Ser A Math Phys Sci [Internet]. 1955 Jul 12 [cited 2020 Sep 11];230(1183):531–48. Available from: https://royalsocietypublishing.org/doi/10.1098/rspa.1955.0149

[10] SHINNO H, KOIZUMI T, ITO Y. Analysis of Damped Vibration of the System with the Contact Surface : 1st Report, Case of the Consideration of Micro-Slip. Trans Japan Soc Mech Eng Ser C. 1983;49(448):2110–5.

[11] YOSHIDA T. Free Rolling Friction and Properties of Material. J Japan Soc Precis Eng. 1961;27(318):468–72.

[12] TANAKA T, OIWA T, OTSUKA J, ONDA H. Study on Linear Ball Guideway for Precision Positioning. J Japan Soc Precis Eng. 2007;73(3):350–4.

[13] Nozomu Y, Sumio S, Yasuto T, Takeko M, Syunichi S. Effect of hysteretic damping characteristics on earthquake response of ground. Proc JSCE Earthq Eng Symp. 2003;27:113–20.

[14] Muravskii G. On description of hysteretic behaviour of materials. Int J Solids Struct. 2005;42(9–10):2625–44.

[15] Olsson H, Åström KJ, Canudas De Wit C, Gäfvert M, Lischinsky P. Friction Models and Friction Compensation. Eur J Control. 1998;4(3):176–95.

[16] Piatkowski T. GMS friction model approximation. Mech Mach Theory [Internet]. 2014;75:1–11. Available from: http://dx.doi.org/10.1016/j.mechmachtheory.2014.01.009

[17] Al-Bender F, Symens W. Dynamic characterization of hysteresis elements in mechanical systems. I. Theoretical analysis. Chaos [Internet]. 2005 Mar 24 [cited 2020 Sep 11];15(1):013105. Available from: http://aip.scitation.org/doi/10.1063/1.1844991

[18] SAKAI Y, TANAKA T, TSUTSUMI M. Influence of the Excitation Force Amplitude on Vibration Characteristics of a Linear Rolling Bearing. J Japan Soc Precis Eng. 2014;80(8):783–91.

[19] Sakai Y, Tanaka T, Yoshioka H. Influence of nonlinear spring behavior of friction on dynamic characteristics of a rolling guideway. J Adv Mech Des Syst Manuf Influ. 2015;9(1):1–15.

[20] Kim TC, Rook TE, Singh R. Super- and sub-harmonic response calculations for a torsional system with clearance nonlinearity using the harmonic balance method. J Sound Vib [Internet]. 2005 Mar 1;281:965–93. Available from: https://ui.adsabs.harvard.edu/abs/2005JSV...281..965K

[21] KAKINO Y. A Study on the motion accuracy of NC machine tools (7th report)-measurement of motion accuracy of 5-axis machine by DBB tests. J Jpn Soc Precis Eng [Internet]. 1994;60(5):718–23. Available from: https://ci.nii.ac.jp/naid/10029041186/

[22] Ohashi T, Shibata H, Futami S, Kishi H, Sato R. Influence of linear ball guide preloads and retainers on the microscopic motions of a feed-drive system. J Adv Mech Des Syst Manuf. 2018;12(5):1–10.

[23] Yi Y, Kim YY, Choi JS, Yoo J, Lee DJ, Lee SW, et al. Dynamic analysis of a linear motion guide having rolling elements for precision positioning devices. J Mech Sci Technol. 2008;22:50–60.

[24] Ohta H, Hayashi E. Vibration of linear rolling guideway type recirculating linear ball bearings. J Sound Vib. 2000;235:847–61.

[25] Rahman M, Mansur MA, Lee LK, Lum JK. Development of a polymer impregnated concrete damping carriage for linear guideways for machine tools. Int J Mach Tools Manuf. 2001;41(3):431–41.

[26] Sakai Y, Tanaka T. Influence of lubricant on nonlinear vibration characteristics of linear rolling guideway. Tribol Int [Internet]. 2020;144(December 2019):106124. Available from: https://doi.org/10.1016/j.triboint.2019.106124

[27] Ohta H. Sound of Linear Guideway Type Recirculating Linear Ball Bearings. Trans Am Soc Mech Eng. 2017;121(October 1999).

[28] SAKAI Y, TSUTSUMI M. Dynamic Characteristics of Linear Rolling Bearings for Machine Tools. J Mach Eng. 2013;13(3).